TRENDS IN SCIENCES 2026; 23(5): 12125
https://doi.org/10.48048/tis.2026.12125 RESEARCH ARTICLE

Multi-Target AntiAging Potential of *Sterculia Populifolia* DC Stem Bark: Inhibition of Tyrosinase, Elastase, and Hyaluronidase, LC–MS/MS Profiling and Molecular Docking

Nur Khairi[1,*], Nursamsiar Nursamsiar[2], Novi Fajar Utami[3], Syamsu Nur[2], Marwati Marwati[4] and Maulita Indrisari [5]

[1]*Department of Pharmaceutical and Technology, Universitas Almarisah Madani, Makassar 48201, Indonesia*
[2]*Department of Pharmaceutical Chemistry, Universitas Almarisah Madani, Makassar 48201, Indonesia*
[3]*Department of Pharmacy, Faculty of Mathematics and Natural Sciences, Universitas Pakuan, Bogor 16143, Indonesia*
[4]*Department of Pharmaceutical Biology, Universitas Almarisah Madani, Makassar 48201, Indonesia*
[5]*Department of Pharmacotherapy, Faculty of Medicine, Universitas Palangka Raya, Palangkaraya 73111, Indonesia*

([*]Corresponding author's e-mail: nurkhairijalil@gmail.com)

Received: 30 September 2025, Revised: 12 November 2025, Accepted: 22 November 2025, Published: 10 January 2026

Abstract

This study evaluates the stem bark of *Sterculia populifolia* as a multi-target anti-aging cosmeceutical source, aiming to map its phytochemical profile and assess tyrosinase, elastase, and hyaluronidase inhibition integrated with molecular docking and LCMS/MS. Solvent-guided extraction (n-hexane, ethyl acetate, ethanol) was followed by phytochemical screening, LCMS/MS, *in vitro* enzyme assays against the three targets, and residue-level docking; integration of chemical features with bioactivity prioritized extracts and candidate molecules. Ethanol afforded the highest yield and enriched phenolic and heteroatom-rich constituents, aligning with the strongest tyrosinase inhibition; n-hexane concentrated lipophiles that produced the most pronounced anti-elastase effect, while hyaluronidase inhibition was moderate. Docking substantiated residue-level rationales: For tyrosinase, stearidonic acid, 4-[(E)-(3,5-diamino-1H-pyrazol-4-yl)diazenyl]phenol, N~4~-(4-methoxyphenyl)-5-nitro-N~2~-(tetrahydrofuran-2-ylmethyl)pyrimidine-2,4,6-triamine, and 6-Guanidinohexanoic acid Hemihydrate engaged copper-proximal, histidine-rich regions. For elastase, 5,5′-(1,3-phenylene)bis[2-(3-(1H-tetrazol-5-yl)propyl)-2H-tetrazole] and the same polyunsaturated fatty acid bridged S1/S2 subsites near His57/Ser195/Gly193. For hyaluronidase, ethyl 2-(3,5-dimethyl-1H-pyrazol-1-yl)-4-[(6-methyl-2-phenylpyrimidin-4-yl)hydrazinyl]pyrimidine-5-carboxylate and stearidonic acid occupied the substrate-binding loop, although solution-phase potency remained limited. These patterns mirror solvent selectivity and explain the anti-enzyme hierarchy; integrating chemistry with bioactivity strengthens the multi-target cosmeceutical prospect and underscores the need for enrichment and formulation to maximize hyaluronidase effects. Overall, ethanol extracts are prioritized for pigmentation control via tyrosinase, and n-hexane extracts for matrix protection via anti-elastase, while further bioassay-guided extraction, structure authentication, cellular and *in vivo* testing, and formulation optimization are warranted for translational development.

Keywords: *Sterculia populifolia*, Molecular docking, Tyrosinase inhibition, Elastase inhibition, Hyaluronidase inhibition, LCS/MS, Antiaging

Introduction

The stem bark of *Sterculia populifolia* DC is a promising anti-aging candidate. Its wood derived bioactive architecture—predominantly phenolics, flavonoids, and terpenoids—has been widely implicated

in targeting key cutaneous enzymes and dysregulated pigmentation pathways, notably tyrosinase, elastase, and hyaluronidase. Previous investigations have reported anti-aging potential for this species; however, those studies relied primarily on ethanolic extracts and did not employ a solvent-guided extraction strategy to comprehensively map the bark's bioactivity across solvents of differing polariy [1-4]. Pharmacological justification for this claim rests on a substantial body of literature showing that natural-product inhibitors can suppress melanogenesis, reduce extracellular matrix (ECM) proteolysis, and preserve hyaluronic acid (HA), thereby addressing hyperpigmentation, wrinkle formation, and declines in skin hydration [5-7]. In parallel, advances in molecular docking and analytical chemical profiling have enabled residue-level mapping of ligand–enzyme interactions and the linking of plant extract to dermatologically relevant biological endpoints [8-9].

As an anti-aging candidate, *S. populifolia* stem bark is further supported by the multi-target strategy now common in nature-derived cosmeceuticals: Inhibition of tyrosinase to diminish melanin formation, suppression of elastase to protect elastic fibers, and modulation of hyaluronidase to maintain dermal HA. Evidence across plant systems shows that benchmark depigmenting agents such as kojic acid and arbutin, together with diverse phenolics and flavonoids, inhibit tyrosinase, while selected polyphenols/terpenoids suppress elastase and several flavonoids and saponins modulate hyaluronidase [10-12]. Consequently, the phytochemical composition typically encountered in bark—and tractable via LC–MS/MS—provides a rational basis for exploring *S. populifolia* as a source of multi-functional anti-aging candidates [13].

To contextualize the anti-aging potential of *S. populifolia*, it is valuable to compare its activity with well-established anti-aging agents such as *Glycine max* (soybean), *Curcuma aromatica* (turmeric), and *Syzygium jambos* (rose apple). Studies have shown that *Glycine max* extracts, particularly those rich in isoflavones, exhibit notable tyrosinase inhibition, which is commonly associated with skin lightening and pigmentation management [14]. Similarly, *Curcuma aromatica* has been recognized for its polyphenolic compounds, which not only inhibit tyrosinase but also suppress elastase activity, aiding in the prevention of wrinkle formation [15]. *Syzygium jambos,* with its high flavonoid content, has demonstrated potential for modulating both elastase and hyaluronidase, improving skin hydration and elasticity [16]. In comparison, *S. populifolia* exhibits promising inhibition of tyrosinase and elastase, with a unique profile in its ability to modulate hyaluronidase activity, positioning it as a multi-functional candidate for anti-aging applications.

A central research problem in this domain is the chemical heterogeneity of plant extracts, which gives rise to emergent activity patterns such that bulk metrics like total phenolics or total flavonoids do not necessarily predict enzymatic potency. This consideration is critical for *S. populifolia*, because the success of a stem bark-derived anti-aging candidate depends on the integration of extraction technique, profiling resolution, and mechanistic confirmation [4]. Differences in extraction practice shift the apparent bioactivity landscape by selectively recovering polar versus lipophilic classes, while variability in enzyme isoforms and assay conditions further complicates cross-study comparisons—particularly for hyaluronidase, where substrate composition and cofactors can strongly influence apparent inhibitory potency [17].

A commonly adopted solution is an integrated pipeline that combines solvent-guided extraction, LC–MS/MS profiling to link mass features with bioactive extracts, and docking to generate residue-level binding hypotheses testable in enzyme bioassays [18,19]. For *S. populifolia*, such an approach enables mapping of the relative contributions of phenolics and terpenoids to the suppression of tyrosinase, elastase, and hyaluronidase, thereby improving the accuracy of fraction/component prioritization. Specific evidence from prior work underscores that phenolic-based tyrosinase inhibitors—including condensed tannins and multiple flavonoids—show consistent affinity for the dicopper center of tyrosinase and conserved histidine residues, explaining competitive or mixed-type inhibition modes [10,12]. By mechanistic analogy, phenolic-enriched extracts from *S. populifolia* stem bark can reasonably be expected to contribute to melanogenesis inhibition relevant to anti-aging indications linked to dyschromia [4].

Beyond pigmentation control, the elastase literature shows that plant-derived polyphenols and terpenoids can limit ECM proteolysis and, in some cases, [20,21]. Accordingly, the more non-polar extracts

of *S. populifolia* stem bark—potentially enriching terpenoids and allied lipophiles—are rationally positioned as anti-elastase candidates that complement depigmenting effects.In the hyaluronidase dimension, evidence that flavonoids (e.g., quercetin) and tomato saponins suppress HA degradation and improve skin hydration/texture, together with indications of benefit for wound healing and allergic response modulation, adds further rationale that selected *S. populifolia* extracts may contribute to preservation of dermal hydration—a key component of anti-aging effects [22,23]. Although potency at the crude-extract level may appear modest, docking provides a framework for mapping candidate features and improving the likelihood of success through formulation and enrichment.

An overview of closely related literature reveals a coherent thread: First, extraction and solvent selection determine the composition of bioactives and the measurable enzymatic signals [24,25] second, LC–MS/MS effectively links extracts/mass features with biological phenotypes and guides iterative enrichment [18]; and third, docking—including advanced approaches such as CDOCKER—generates active-site binding hypotheses aligned with reference inhibitor data. The remaining gap is the need for studies that simultaneously map chemical composition, predict binding modes across the three principal cutaneous enzymes, and validate activity under harmonized conditions, so that multi-target inference is robust and translatable [26].

Guided by this rationale, the present study positions *S. populifolia* stem bark as a multi-functional anti-aging candidate and evaluates its potential through an integrated framework of solvent-guided extraction, LC–MS/MS profiling, and molecular docking linked to quantitative enzyme assays for tyrosinase, elastase, and hyaluronidase. Our objectives are to test the hypothesis that medium- to high-polarity extracts from *S. populifolia* more effectively inhibit tyrosinase, whereas more non-polar extracts more effectively suppress elastase; assess whether indications of hyaluronidase inhibition can be rationalized at the feature level via docking; and present a coherent mechanistic narrative from chemical space to clinically relevant bioactivity [27]. The study's novelty lies in the explicit alignment of three cutaneous enzyme targets within a single pipeline anchored in LC–MS/MS and residue-resolved docking, thereby strengthening traceability between mass-based annotations, active-site interaction hypotheses, and bioassay outcomes, and reinforcing the justification for *S. populifolia* as an anti-aging candidate amenable to further optimization.

Materials and methods

Sample processing and extraction

The stem bark of Sterculia populifolia was collected from Kupang, East Nusa Tenggara, Indonesia, with a total weight of 5 kg. After thorough cleaning and washing to remove impurities, the material was dried in a drying cabinet at 50 °C and subsequently ground into a fine powder. A successive maceration procedure was employed using n-hexane, ethyl acetate, and 96% ethanol as solvents, with a solvent-to-sample ratio of 1:7 (v/v). For each solvent step, the powdered material was immersed and occasionally agitated, after which the mixture was filtered to separate the liquid extract (macerate) from the solid residue.The collected macerates were stored in light-protected conditions, while the residues underwent repeated maceration under the same conditions until the solvent became colorless. Combined macerates were concentrated under reduced pressure using a rotary evaporator at 50 °C. The resulting viscous extracts were then transferred into suitable containers and further dried in an oven at 50 °C to obtain concentrated crude extracts, from which the yields were calculated. The dried extracts were stored at 4 °C until further use [1-3].

Tyrosinase enzyme inhibition activity

A spectrophotometric assay was employed to evaluate the anti-aging potential of the samples by measuring their ability to inhibit tyrosinase activity, following previously reported methods with slightmodifications. L-3,4-dihydroxyphenylalanine (L-DOPA) and kojic acid were used as the substrate and positive control, respectively. The extracts were prepared in a concentration range of 12.5 - 400 µg/mL. For each reaction, 30 µL of extract was mixed with 125 µL of phosphate buffer (0.1 M, pH 6.8) and 5 µL of tyrosinase enzyme solution (2,500 U/mL). The mixture was incubated at 37 °C for 30 min, after which 40 µL of L-DOPA (2.5 mM) was added to initiate the reaction.Absorbance was measured at 515 nm, with

additional readings taken for the solvent blank and kojic acid as the positive control. The percentage of tyrosinase inhibition was determined using a linear regression model y = a+bx, where a and b are the regression coefficients, x represents the extract concentration, and y indicates the calculated inhibition percentage [28-32].

Elastase inhibition assay

The anti-aging potential of the sterculia populifolia extracts was determined by evaluating their ability to inhibit elastase using an enzymatic colorimetric method. In this assay, the interaction between elastase and the synthetic substrate N-succinyl-Ala-Ala-Ala-p-nitroanilide (SANA) produces a yellow-colored product, whose absorbance was measured at 405 nm using a microplate reader (Glomax GM 3000, Promega, USA). For each reaction, 30 µL of extract solution (10 - 1,000 µg/mL) was combined with 15 µL of elastase enzyme (4 U/mL) in a 96-well microplate containing Tris-HCl buffer (pH 8.0). The mixture was incubated for 10 min at 25 °C. Subsequently, 30 µL of the substrate solution (1.3 mM SANA) was added, and incubation was continued at 25 °C for an additional 50 min using a Memmert IN55 incubator. After incubation, the absorbance of the reaction mixture was recorded at 405 nm. The elastase inhibitory activity of each samples was expressed as the IC_{50} value (the concentration required to inhibit 50% of enzyme activity) [33,34]. Quercetin was employed as a positive control, and all assays were performed in triplicate (n = 3) to ensure reproducibility.

Hyaluronidase inhibition assay

The hyaluronidase inhibitory activity was evaluated using a colorimetric microplate method. In each well, 50 µL of sample solution was mixed with 75 µL of hyaluronidase enzyme and incubated at 37 °C for 10 min. After the initial incubation, 75 µL of hyaluronic acid substrate was added, followed by a second incubation at 37 °C for 45 min. Subsequently, 100 µL of bovine serum albumin (BSA) solution was introduced, and the mixture was incubated again for 3 min. After the final incubation, the absorbance was measured at 600 nm using a microplate reader. A control reaction (blank) was prepared in the same manner but without the test sample, containing 100 µL phosphate buffer (pH 7.0), 75 µL hyaluronidase enzyme, 75 µL hyaluronic acid substrate, and 100 µL BSA solution [32,34]. All experiments were performed in triplicate (n = 3) to ensure reproducibility.

LC–MS/MS analysis

The bioactive constituents of the samples were analyzed using a high-performance liquid chromatography–mass spectrometry (LC–MS/MS) system. Chromatographic separation was performed on an ACQUITY UPLC® H-Class System (Waters, USA) coupled to a Xevo G2-S QTof mass spectrometer (Waters, USA). The mobile phase consisted of water containing 5 mM ammonium formate (phase A) and acetonitrile with 0.05% formic acid (phase B), delivered at a flow rate of 0.2 mL/min under a step-gradient program for 23 min. The injection volume was 5 µL, with all samples pre-filtered through a 0.2 µm syringe filter prior to analysis. Mass spectrometric detection was performed using electrospray ionization (ESI) in positive ion mode. Data acquisition and subsequent processing were carried out using MassLynx software (version 4.1) [18,19].

Molecular docking study

Molecular docking was performed to investigate the binding interactions between selected compounds and the enzymes tyrosinase, elastase, and hyaluronidase using AutoDock Vina v1.1.2 (The Scripps Research Institute, La Jolla, San Diego, CA, USA) [19]. The three-dimensional (3D) structures of tyrosinase (PDB CID: 5M8N), elastase (PDB CID: 1BRU), and hyaluronidase (PDB CID: 5YDI) were retrieved from the RCSB Protein Data Bank (http://www.rcsb.org; accessed on December 20, 2024). The chemical structures of the selected ligands were downloaded from PubChem (http://pubchem.ncbi.nlm.nih.gov; accessed on December 20, 2024). Input files for proteins and ligands were prepared using AutoDock Tools v1.5.6 (ADT; Scripps Research Institute, La Jolla, San Diego, CA, USA). Protein preparation included the removal of water molecules and the addition of non-polar hydrogen atoms. Each target protein was re-docked to validate the docking protocol. The validation produced RMSD values of 1.52 Å for elastase (grid box size: 4×60×46; coordinates: 69.048×51.487×55.179), 1.67 Å for tyrosinase (grid box size: 30×30×22; coordinates: 16.34×5.955×25.418), and 1.22 Å for hyaluronidase

(grid box size: 40×30×28; coordinates: –10.482×–69.52×53.708). These RMSD values fall within the acceptable threshold for molecular docking validation, confirming that the method is reliable and suitable for subsequent re-docking of compound molecules

The docking accuracy was enhanced by setting the exhaustiveness parameter to 300. After docking simulations, the best-scoring binding poses were selected and visualized using PyMOL v1.7.6 (DeLano Scientific LLC, Palo Alto, CA, USA; http://www.pymol.org; accessed on December 20, 2024). Protein–ligand interactions were further analyzed using BIOVIA Discovery Studio Visualizer v21.1.0.0 (Accelrys, San Diego, CA, USA; https://discover.3ds.com/discovery-studio-visualizer-download; accessed on December 20, 2024) [28,35,36].

The selection of compound for docking studies was based on several criteria, including LC-MS/MS intensity, structural diversity and precedence in the literature. Compounds with higher LC-MS/MS intensity were prioritized, as the are likely to be the dominant bioactive components in the extract. Additionally, structural diversity was considered to ensure the representation of various types of interactions within the enzyme active site. Compounds previously reported in the literature as inhibitors of tyrosinase, elastase and hyluronidase were also included to strengthen the mechanistic validation of the study.

Statistical analysis

All statistical analyses were conducted using IBM SPPS Statistics for Windows, Version 20.0 (IBM Corp., Armonk, NY, USA). Prior to further statistical tests, data were assessed for normality using the Shapiro-Wilk test. Since the data were normally distributed, one-way ANOVA was used to compare differences between treatment groups. When significant were found by ANOVA, a Tukey post-hoc test wes performed to identify which specific groups were significantly different.

Results and discussion

Solvent-guided extraction of the stem bark of *Sterculia populifolia* produced clear differences in both crude yield and phytochemical composition across the obtained extracts (**Table 1**). The ethanolic extract afforded the highest yield, followed by ethyl acetate and *n*-hexane, consistent with the established principle that increasing solvent polarity enhances the recovery of medium- to high-polarity constituents such as polyphenols and glycosides, whereas non-polar solvents preferentially enrich lipophilic compounds, including terpenoids [37,38]. Qualitative phytochemical screening confirmed the presence of phenolics/tannins, flavonoids, alkaloids, and steroids/terpenoids in all three extracts, with phenolic–flavonoid signatures appearing relatively more pronounced in the ethyl acetate and ethanol extracts (**Table 2**). These findings align with previous reports emphasizing that solvent selection dictates both the class selectivity and downstream bioactivity potential of plant-derived extracts [39,40]. Further class-level quantification revealed that total phenolic content (TPC) and total flavonoid content (TFC) were generally higher in the ethyl acetate and ethanol extracts, while *n*-hexane remained comparatively low—an extraction pattern that will serve to contextualize the subsequent enzyme-targeted evaluations, while acknowledging that bulk compositional metrics alone do not always predict functional potency in complex multiconstituent mixtures [41].

Table 1 Result %yield, TPC and TFC of *Sterculia populifolia* DC.

Solvent	Extraction yield (%)	TPC (mg GAE/g of extract)	TFC (mg QE/g extract)
n-hexane	5.2	0.81 ± 2.37	7.2 ± 3.69
Ethyl acetate	8.1	1.40 ± 5.49	25.75 ± 4.52
Ethanol 96%	13.6	1.09 ± 3.95	18.78 ± 3.17

Table 2 Thin layer chromatography (TLC) confirmation results.

Compound	Reagent	Visible observation after spraying	Solvent			Colour
			n-hexane	Ethyl acetat	Ethanol 96%	
Alkaloids	Dragendorff	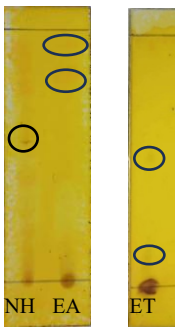	+	+	+	Brown and Orange spots
Flavonoids	Ammonia	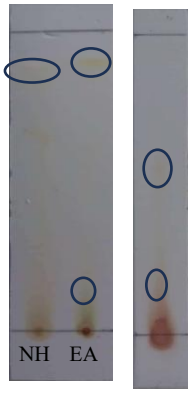	+	+	+	Yellow and brown spots
Tanins/ Fenolics	FeCl3		+	+	+	Black spots

Compound	Reagent	Visible observation after spraying	Solvent		Colour	
			n-hexane	Ethyl acetat	Ethanol 96%	
Steroids dan Terpenoids	Lieberman-Burchard	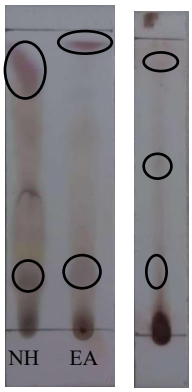	+	+	+	Purple spots

Among the tested extracts, the ethanolic extract showed the strongest tyrosinase inhibition (IC_{50} = 513.80 ± 3.75 µg/mL), followed by ethyl acetate (IC_{50} = 1.006.43 ± 13.38 µg/mL) and n-hexane (IC_{50} = 2.541.12 ± 3.25 µg/mL), whereas the positive control kojic acid exhibited an IC_{50}= 5.55 ± 0.54 µg/mL. The ethanolic extract exhibited the strongest tyrosinase inhibition among the tested fractions, outperforming the ethyl acetate and n-hexane extracts across the evaluated concentration range. This was reflected in the sigmoidal concentration–response curves and the lowest IC_{50} value observed for ethanol. Nevertheless, the potency of the fractions remained above the sub-10 µg/mL range typically achieved by kojic acid, a copper-chelating standard employed here as a positive control. The potency trend (ethanol > ethyl acetate ≫ n-hexane) mirrors the enrichment of phenolic and flavonoid constituents and aligns with the consensus that phenolic frameworks and nitrogen-containing aromatic scaffolds exhibit favorable shape and chemical complementarity toward the dicopper active site of tyrosinase [42]. In contrast, the weak activity of the n-hexane fraction is consistent with its lipophilic dominance, which is suboptimal for competing within the mixed hydrophobic–polar active pocket. These findings reinforce the translational framework suggesting that phenolic-rich fractions hold potential for modulating melanogenesis, supporting their relevance for managing hyperpigmentation disorders [43,44].

Table 3 Tyrosinase inhibitory activity.

Solvent	Consentration (µg/mL)					Nilai IC_{50} (µg/mL)
	62.5	125	250	500	1000	
n-Hexane	7.36 ± 2.02	14.87 ± 7.69	17.49 ± 4.57	22.03 ± 7.87	24.57 ±1.53	2541.12 ± 3.25 [d]
Ethyl acetat	4.69 ± 4.13	6.04 ± 2.10	15.38 ± 4.84	36.38 ± 1.94	45.36 ± 2.10	1006.43 ± 13.38 [c]
96% ethanol	18.19 ± 1.88	30.69 ± 5.99	47.59 ± 2.13	53.93 ± 4.52	69.25 ± 0.90	513.80 ± 3.75 [b]
Kojic acid						5.55 ± 0,54[a]

All data were shown as mean ± SD; each treatment was repeated 3 times.
[a,b,c,d] indicate significant difference with Tukey analysis (*p-value* < 0.05, n = 3).
Kojic acid was used as a positive control with concentrations of 4, 6, 8, 10 and 12 µg/mL.

In the elastase assay, the n-hexane extract was the most potent (IC_{50} = 100.09 ± 5.27 µg/mL), followed by ethanol (IC_{50} = 146.87 ± 1.54 µg/mL) and ethyl acetate (IC_{50} = 254.76 ± 4.86 µg/mL); the positive control quercetin yielded an IC_{50} = 4.88 ± 0.69 µg/mL. In contrast to the pattern observed for tyrosinase, the elastase assay revealed that the n-hexane extract exhibited the highest inhibitory potency, followed by

ethanol and ethyl acetate. The concentration–response curves showed a consistent leftward shift for n-hexane, indicating stronger inhibition at lower concentrations. This finding aligns with literature identifying lipophilic polyphenols and terpenoids as effective modulators of serine proteases through interactions with hydrophobic subsites surrounding the catalytic triad and oxyanion hole, with functional implications for mitigating extracellular matrix degradation and wrinkle formation [45-48]. The reported link between elastase suppression and improvements in skin biomechanical parameters in UV-exposed models—including wrinkle reduction—provides translational context for the observed potency trend among the fractions [49] Accordingly, the more pronounced anti-elastase activity of the n-hexane extract complements the depigmenting effects of polar extracts, together supporting a multitarget anti-aging rationale.

Table 4 Elastase inhibitory activity.

Solvent	Consentration (µg/mL)					Nilai IC_{50} (µg/mL)
	46.87	**93.75**	**187.5**	**375**	**750**	
n-Hexane	15.11 ± 11.72	64.67 ± 1.88	73.76 ± 4.38	69.83 ± 5.3	77.36 ±9.45	100.09 ± 5.27[b]
Ethyl acetat	15.99 ± 1.85	42.18 ± 8.90	53.35 ± 1.58	68.42 ± 5.70	79.83 ± 3.91	254.76 ± 4.86[c]
96% ethanol	66.47 ± 0.77	69.14 ± 1.61	73.18 ± 0.58	78.47 ± 1.50	82.07 ± 2.16	146.87 ± 1.54[b]
Quarcetin						4.88 ± 0.69[a]

All data were shown as mean ±SD; each treatment was repeated 3 times.

[a,b,c,d] indicate significant difference with Tukey analysis (*p-value* < 0.05, n = 3).

Quarcetin was used as a positive control with concentrations of 1.5; 4.5; 7.5; 10.5 and 13.5 µg/mL.

In the hyaluronidase (HAase) assay, the ethanolic extract achieved 25.33 ± 2.18% inhibition, the ethyl acetate extract 5.71 ± 3.04% and the n-hexane extract 0%. all three extracts exhibited relatively limited inhibitory effects, even at higher concentration ranges, with the ethanolic extract performing slightly better than ethyl acetate and n-hexane, which were near baseline. This moderate potency should be interpreted within the context that HAase assays are highly sensitive to substrate composition, ionic milieu, and the specific enzyme isoform employed; these factors have been reported to significantly shift potency estimations [50-52]. Nevertheless, the literature highlights that flavonoids such as quercetin and tomato-derived saponins can act as competitive HAase inhibitors, helping to preserve dermal hyaluronic acid, enhance skin hydration and texture, and contribute to wound healing as well as modulation of allergic responses [32,34]. Within this framework, the modest potency observed at the crude extract level does not preclude potential activity at the constituent level—as suggested by molecular docking studies—or the possibility of enhanced effects through optimized formulation strategies.

Table 5 Hyaluronidase inhibitor activity.

Solvent	Consentration(µg/mL)	% Inhibition
n-Hexane	1.250	0
Ethyl acetat	1.250	5.71 ± 3.04
96% ethanol	1.250	25.33 ± 2.18

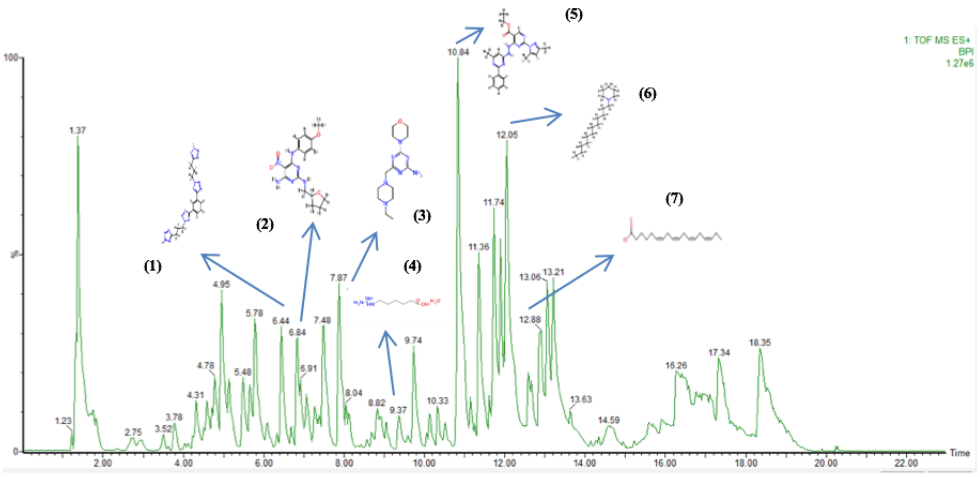

Figure 1 LC-MS/MS profile ethanolic extract *S.populifolia* stem bark.

The peak numbers in the chromatogram (Peak 1, Peak 2, etc.) correspond to the compounds listed in **Table 6**.

Table 6 Identified phytocompounds from LC.MS/MS analysis.

No	Retention time (min)	Observed MS (m/z)	Molecular ion	Compound name	Molecular formula
1	6.44	435.20	M+H	5,5′-(1,3-Phenylene)bis{2-[3-(2H-tetrazol-5-yl)propyl]-2H-tetrazole}	$C_{16}H_{18}N_{16}$
2	6.84	361.16	M+H	N~4~-(4-methoxyphenyl)-5-nitro-N~2~-(tetrahydrofuran-2-ylmethyl)pyrimidine-2,4,6-triamine	$C_{16}H_{20}N_6O_4$
3	7.87	308.22	M+H	4-[(4-Ethyl-1-piperazinyl)methyl]-6-(4-morpholinyl)-1,3,5-triazin-2-amine	$C_{14}H_{25}N_7O$
4	9.37	192.13	M+H	6-Guanidinohexanoic Acid Hemihydrate	$C_7H_{17}N_3O_3$
5	10.84	445.21	M+H	Ethyl 2-(3,5-dimethyl-1H-pyrazol-1-yl)-4-[2-(6-methyl-2-phenyl-4-pyrimidinyl)hydrazino]-5-pyrimidinecarboxylate	$C_{23}H_{24}N_8O_2$
6	12.05	254.28	M+H	N-Dodecylpiperidine	$C_{17}H_{15}N$
7	12.88	277.21	M+H	Stearidonic acid	$C_{18}H_{28}O_2$

Docking analyses support the biochemical findings by revealing that several annotated constituents from the ethanolic extract interact with key residues in the tyrosinase active site. Notably, contacts with His192, His215, His377, and His381—critical for coordinating the binuclear copper cluster—align with established mechanisms of competitive or mixed-type inhibition, as seen with reference inhibitors like kojic acid and chlorogenic acid [30,36]. Among the docked compounds, stearidonic acid exhibited a relatively favorable score, while diazinyl-phenol and guanidinohexanoic acid formed stable complexes

involving Thr391, Gly389, Asn378, and adjacent histidines 9 (**Figure 2**). Although fatty acids are atypical tyrosinase inhibitors, their shape complementarity and hydrophobic/hydrogen-bonding interactions can yield meaningful binding energies. In contrast, phenolic and heteroatom-rich scaffolds—such as flavonoids and tannins—are more consistent with literature-reported structure–activity relationships [53,54].

The alignment of docked poses with residues like Arg374, Asn378, and Leu382, combined with TLC-confirmed phenolic content, suggests that polyphenolic constituents are likely contributors to the observed inhibitory activity. This is further supported by the ethanol fraction's superior IC_{50}, positioning these compounds as promising leads for downstream biochemical and cellular investigations. While gene-level modulation was not assessed, the observed active-site engagement and copper-proximal binding modes reinforce the relevance of these constituents for dermatologic applications targeting hyperpigmentation disorders such as melasma and solar lentigines. The therapeutic appeal of plant-derived inhibitors remains high, especially given the safety concerns surrounding synthetic agents and the benchmark efficacy of kojic acid and arbutin [55,56].

Table 7 Docking score and binding sites of the different ligants with tyrosinase.

Compound	Score (Kcal/mol)	Active site residues involved in H-Bond
Narative ligan	**–6.41**	TYR363, GLY388, ARG374, SER394, LEU382, HIS377, HIS215, HIS192, GLY389, ASN378, THR391, HIS381, GLN390
5,5'(1,3-Phenylene)bis{2-[3-2H-tetrazol—5-yl)propyl]-2H-tetrazole}	–4.56	ASN378, GLY388, THR39, HIS377, ARG374
Stearidonic acid	**–8.73**	GLY389, SER394, THR391, LEU382, HIS381, ARG374
4-[(E)-(3,5-Diamino-1H-pyrazol-4-yl)diazinyl}phenol	**–7.00**	THR391, GLY389, HIS192, ASN378, LEU382, GLN390
N~4~-(4-methoxyphenyl)-5-nitro-N~2~-(tetrahydrofuran-2-ylmet	**–7.08**	ARG374, ASN378, HIS381, SER394, HIS192, HIS377
6-Guanidinohexanoic acid Hemihydrate	**–7.44**	THR390, ASN378, SER394, HIS192, HIS381, HIS215, TYR362
Ethyl 2-(3,5-dimethyl-1H-pyrazol-1-yl)-4-[2-6 methyl-2-phenyl-pyrimidinyl)hydrazine]-5-pyrimidinecarboxylate	–5.38	ARG374, ASN378, HIS215
N-Dodecylpiperidine	–4.65	LEU382, HIS381, HIS377, HIS215

In contrast, elastase inhibition was most pronounced in the n-hexane extract, which yielded the lowest IC_{50}, followed by ethanol and ethyl acetate. This reversed polarity relative to tyrosinase inhibition reflects the known role of lipophilic scaffolds—particularly terpenoids and long-chain moieties—in modulating serine proteases and mitigating photoaging-related ECM degradation. Docking results corroborate this trend, showing ligand interactions with His57, Ser195, and Gly193—residues central to the catalytic triad and oxyanion hole. Ethanolic constituents such as stearidonic acid and nitrogenous heterocycles bridged the S1/S2 subsites, stabilized by π-stacking, van der Waals forces, and hydrogen bonding with Phe192, Phe215, Ser214, and His57. These residue-level contacts mirror docking patterns reported for natural flavonoids and terpenoids with anti-elastase activity [12,28], and the strong assay performance of the nonpolar fraction aligns with literature linking elastase suppression to improved skin elasticity and wrinkle reduction [55].

Table 8 Docking score and binding sites of the different ligants with Elastase.

Compound	Score (Kcal/mol)	Active site residues involved in H-Bond
Narative ligan	**–8.80**	VAL216, HIS57, GLY193, SER195, ARG177, CYS168, LEU167, ASP194, PHE192, PHE215, ARG217, SER215, ARG217, SER214, CYS191
5,5'(1,3-Phenylene)bis{2-[3-2H-tetrazol—5-yl)propyl]-2H-tetrazole	**–7.64**	LEU167, ARG217, VAL216, CYS191, CYS168, PHE215, PHE192, GLY193
Stearidonic acid	**–7.47**	PHE192, VAL216, PHE215, CYS191, SER214, HIS57, ASP194, GLY193
4-[(E)-(3,5-Diamino-1H-pyrazol-4-yl)diazinyl}phenol	–4.87	HIS57, VAL216, SER214
N~4~-(4-methoxyphenyl)-5-nitro-N~2~-(tetrahydrofuran-2-ylmet	–5.58	SER195, GLY193, HIS57, PHE192
6-Guanidinohexanoic acid Hemihydrate	–6.15	SER214, HIS57, CYS191, ASP194
Ethyl 2-(3,5-dimethyl-1H-pyrazol-1-yl)-4-[2-6 methyl-2-phenyl-pyrimidinyl)hydrazine]-5-pyrimidinecarboxylate	–6.79	SER214, SER195, HIS57
N-Dodecylpiperidine	–5.47	VAL216, PHE192, HIS57

Hyaluronidase inhibition was comparatively weak across all extracts, with ethanol showing modest activity and n-hexane negligible. This limited biochemical signal contrasts with favorable docking scores for select annotated molecules that engaged Gly248–Thr252–Lys251 and the His384-adjacent loop. Such discrepancies between docking predictions and assay outcomes are common in systems with isoform diversity and complex substrate environments. While docking reveals thermodynamically plausible interactions, solution-phase assays are influenced by solubility, aggregation, and microenvironmental factors that may dampen apparent potency. Nonetheless, the dermatological relevance of hyaluronidase inhibition—particularly for maintaining dermal hydration and elasticity—is well documented, with flavonoids like quercetin cited as effective inhibitors. Reports of natural products such as liquiritigenin and tomato saponins enhancing skin texture via hyaluronidase modulation lend biological plausibility to these findings, though future work should consider isoform-specific assays and broader therapeutic endpoints including wound healing and allergic response mitigation [54,57].

Table 9 Docking score and binding sites of the different ligants with Hyaluronidase.

Compound	Score (Kcal/mol)	Active site residues involved in H-Bond
Narative ligan	**–8.03**	GLY207, GLY248, THR249, GLY250, LYS251, THR252, LEU253, HIS384, PRO246, PRO247, ASP205, ILE206
5,5'(1,3-Phenylene)bis{2-[3-2H-tetrazol—5-yl)propyl]-2H-tetrazole}	–6.40	THR252, LYS251, GLY250
Stearidonic acid	**–8.71**	LEU253, THR252, GLY250, LYS251, THR249, GLY408, ALA409, GLY248

Compound	Score (Kcal/mol)	Active site residues involved in H-Bond
4-[(E)-(3,5-Diamino-1H-pyrazol-4-yl)diazinyl}phenol	–6.06	GLY248, HIS384
N~4~-(4-methoxyphenyl)-5-nitro-N~2~-(tetrahydrofuran-2-ylmet	–7.18	ALA409, GLY408, THR249
6-Guanidinohexanoic acid Hemihydrate	–5.27	PRO247, LYS251
Ethyl 2-(3,5-dimethyl-1H-pyrazol-1-yl)-4-[2-6 methyl-2-phenyl-pyrimidinyl)hydrazine]-5-pyrimidinecarboxylate	**–8.06**	ASP205, ILE206, GLY207, ALA409, GLY408, THR252, CYS209, ILE380
N-Dodecylpiperidine	–5.78	THR252, GLY250

Docking analyses refine this interpretation by identifying residue-level interactions for specific annotated constituents from the ethanolic extract. In particular stearidonic acid, 4-[(E)-(3,5-diamino-1H-pyrazol-4-yl)diazenyl]phenol, N~4~-(4-methoxyphenyl)-5-nitro-N~2~-(tetrahydrofuran-2-ylmethyl)pyrimidine-2,4,6-triamine, and 6-Guanidinohexanoic acid adopted stable poses engaging the canonical constellation of histidines—His192, His215, His377, and His381—and neighboring residues Arg374/Asn378/Leu382 (**Figure 2**). These contacts are consistent with competitive or mixed-type inhibition that either chelates copper or sterically restricts access to the catecholase site, a pattern well documented for kojic acid and chlorogenic acid [30]. Although long-chain fatty acids are not prototypical tyrosinase inhibitors, stearidonic acid can achieve relevant binding energies through shape complementarity and hydrophobic/H-bond networks within access channels, whereas the phenolic azo scaffold of 4-[(E)-(3,5-diamino-1H-pyrazol-4-yl)diazenyl]phenol and the heteroatom-rich frameworks of the pyrimidine-diamine and 6-(diaminomethylideneamino)hexanoic acid better fit consensus structure–activity relationships in which flavonoids, tannins, and phenolic acids prevail. Mechanistically, suppression of tyrosinase activity directly addresses hyperpigmentation disorders, and plant-derived inhibitors remain clinically attractive vis-à-vis benchmarks such as kojic acid and arbutin. Upstream modulation of melanogenic signaling via MAPK/PI3K pathways is another avenue, though gene-level effects were beyond this study's scope. The present residue-resolved docking, together with the superior ethanolic IC_{50}, nominate these constituents for follow-up in biochemical and cellular systems.

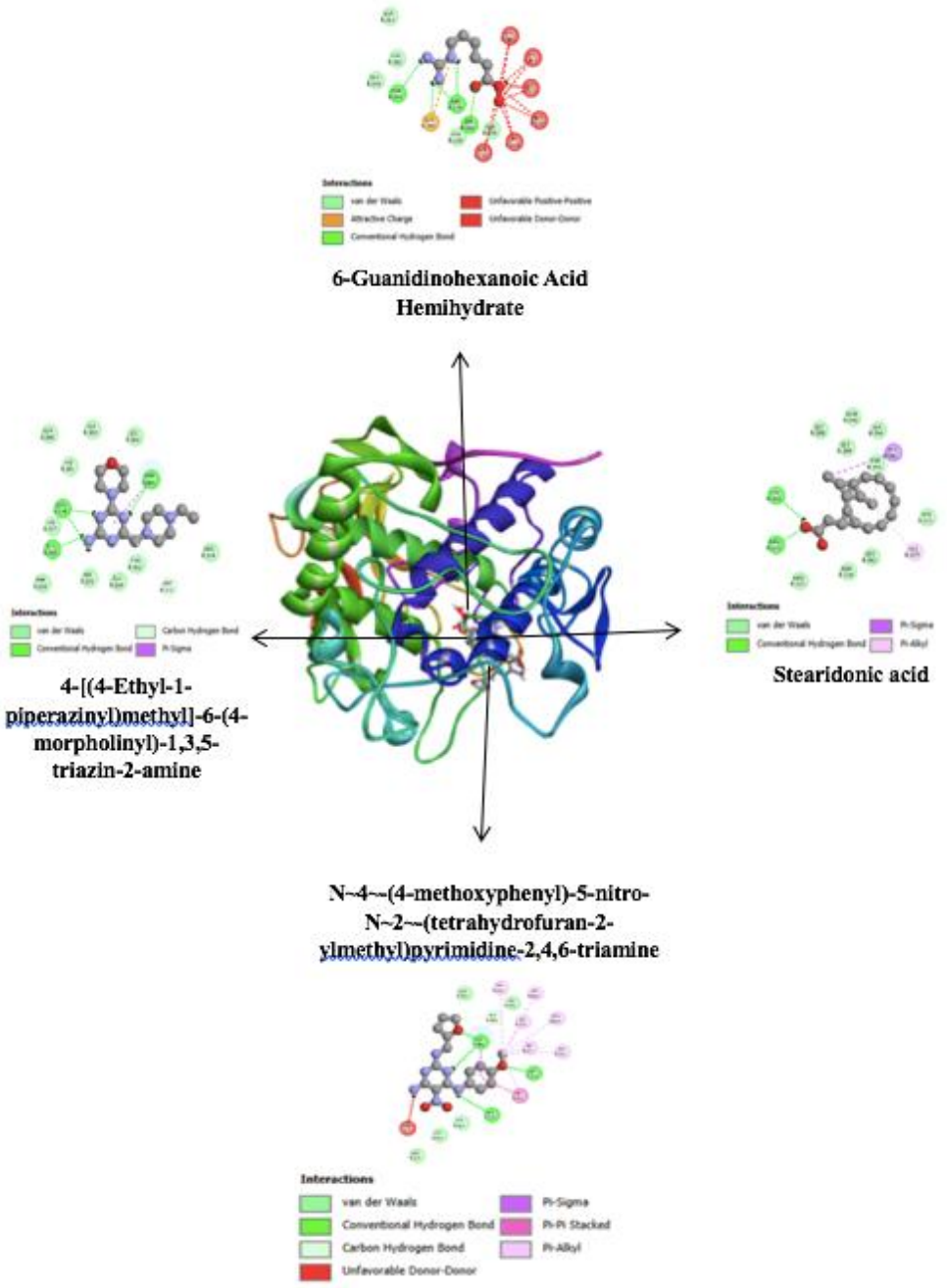

Figure 2 2D and 3D interaction of four ethanolic compounds at the active site of tyrosinase.

In contrast to tyrosinase, elastase inhibition favored the *n*-hexane fraction, with ethanol intermediate and ethyl acetate least active, underscoring the contribution of lipophilic scaffolds to serine-protease modulation [58,59]. Docking converged on catalytically salient regions: 5,5′-(1,3-phenylene)bis[2-(3-(1H-tetrazol-5-yl)propyl)-2H-tetrazole] and stearidonic acid bridged S1/S2 subsites with π/van der Waals packing against Phe192/Phe215, H-bonding via Ser214/Ser195/His57, and proximity to the oxyanion hole (Gly193) (**Figure 3**). The bis-tetrazole affords a dense donor–acceptor array at the pocket entrance, while the polyunsaturated fatty acid blankets hydrophobic patches—an interaction logic compatible with competitive or mixed binding modes reported for natural product–derived elastase inhibitors. Functionally, this molecular picture coheres with dermatologic observations that elastase activity increases under UV stress and that its suppression attenuates wrinkle formation and preserves elasticity [11,13].

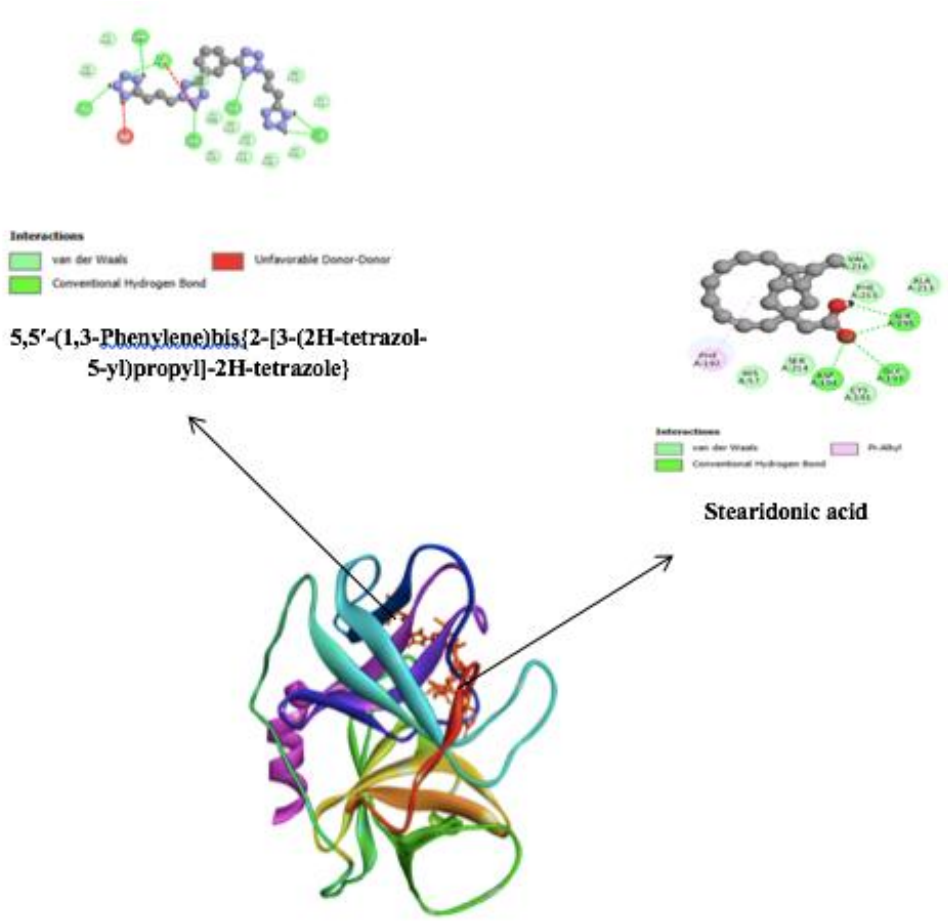

Figure 3 2D and 3D interaction of two ethanolic compounds at the active site of elastase.

At high screening concentrations, hyaluronidase inhibition was limited—ethanol modest, ethyl acetate marginal, and *n*-hexane negligible—yet docking identified plausible complexes at the substrate-binding region. ethyl 2-(3,5-dimethyl-1H-pyrazol-1-yl)-4-[(6-methyl-2-phenylpyrimidin-4-yl)hydrazinyl]pyrimidine-5-carboxylate and stearidonic acid and the loop surrounding His384 (**Figure 4**). Discrepancies between docking favorability and solution-phase potency are not unusual for HAase due to isoform variability, polyanionic substrate dependencies, and potential allosteric sites. Still, the broader literature supports the dermatologic value of HAase inhibition—preserving hyaluronic acid to sustain dermal hydration and elasticity—with flavonoids such as quercetin serving as competitive exemplars. Reports that liquiritigenin and tomato saponins modulate HAase and improve skin texture further reinforce biological plausibility, though assay conditions and isoform selection critically influence measured effects. Beyond aesthetics, HAase modulation intersects wound healing and allergic responses [50,51]. The observed reduction in hyaluronidase activity in S.*populifolia* extract can be further enchanced by formulation strategies aimed at improving the bioavailability and stability of the active compounds. One effective approach is nanoencapsulation, which allows for the encapsulation of active compounds that are prone to degradation or have low solubility into nanocarriers such as nanoparticles or liposomes. Research by Kwon *et al*. [60] demonstrated that nanocapsulation of a *Centella asiatica* crude extract enhanced its hyaluronidase inhibitory activity, which may strengthen its anti-aging potential in topical applications. The nanoencapsulated extract showed a significantly higher inhibitory effect (> 60% inhibition at 0.5 mg/mL) compared to the unencapsulated crude extract [60].

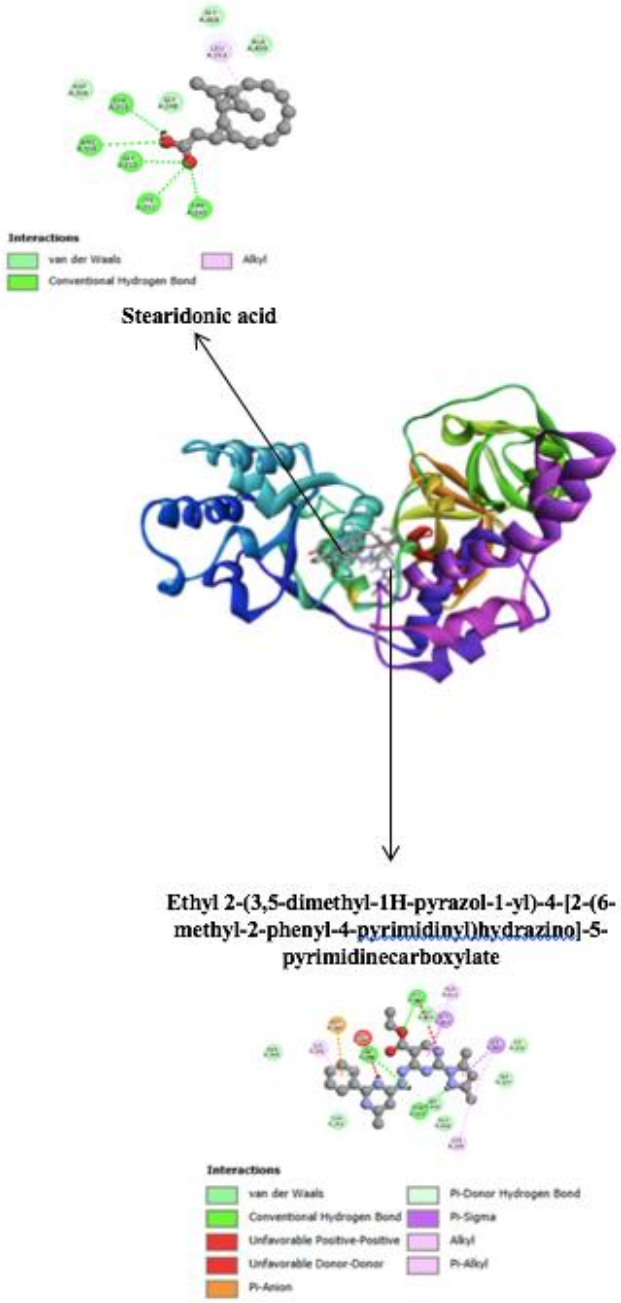

Figure 4 2D and 3D interaction of two ethanolic compounds at the active site of hyluronidase.

Concurrent modulation of tyrosinase, elastase, and hyaluronidase positions *S. populifolia* bark as a multi-functional cosmeceutical candidate with pigmentation-suppressing and photoaging-mitigating potential. Down-modulating tyrosinase directly addresses hyperpigmentation management in line with established clinical targets in melanogenesis. Suppressing elastase intersects with ECM preservation and wrinkle attenuation under UV stress, complementing antioxidant and anti-inflammatory modalities reported for plant-derived polyphenols and terpenoids [27,33,34].

Conclusions

This study positions the stem bark of *Sterculia populifolia* as a promising multi-target cosmeceutical source. Solvent-dependent extraction yielded complementary chemical spaces and activities: Ethanol maximized crude yield and enriched phenolic/heteroatom-rich constituents associated with

the strongest tyrosinase inhibition, whereas n-hexane concentrated lipophiles that drove the most pronounced anti-elastase effect; all fractions showed only modest hyaluronidase inhibition at screening concentrations. LC–MS/MS-anchored molecular docking provided residue-level rationales that align with these bioassays: For tyrosinase, stearidonic acid, 4-[(E)-(3,5-diamino-1H-pyrazol-4-yl)diazenyl]phenol, N~4~-(4-methoxyphenyl)-5-nitro-N~2~-(tetrahydrofuran-2-ylmethyl)pyrimidine-2,4,6-triamine, and 6-Guanidinohexanoic acid Hemihydrate engaged copper-proximal, histidine-rich regions; for elastase, 5,5′-(1,3-phenylene)bis[2-(3-(1H-tetrazol-5-yl)propyl)-2H-tetrazole] and the same polyunsaturated fatty acid bridged S1/S2 subsites near His57/Ser195/Gly193; for hyaluronidase, ethyl 2-(3,5-dimethyl-1H-pyrazol-1-yl)-4-[(6-methyl-2-phenylpyrimidin-4-yl)hydrazinyl]pyrimidine-5-carboxylate and stearidonic acid occupied the Gly248–Thr252–Lys251/His384 region but translated into limited solution-phase potency.

Collectively, these findings support prioritizing phenolic/heteroatom-rich ethanol fractions for pigmentation control via tyrosinase, and lipophilic n-hexane fractions for matrix protection via anti-elastase activity; hyaluronidase modulation may require enrichment and formulation to unmask latent effects. The principal contribution is an integrated, standards-ready framework that links LC–MS/MS features to residue-resolved docking and enzyme outcomes, thereby clarifying lead trajectories from complex extracts. Future work should authenticate structures with reference standards, pursue bioassay-guided fractionation, and advance to cellular and *in vivo* models, including interrogation of melanogenic signaling and isoform-specific hyaluronidase assays, alongside formulation strategies to enhance solubility, delivery, and safety toward translational development.

Acknowledgements

This research was funded by Kementerian Pendidikan, Riset dan Teknologi Indonesia, Direktorat Jenderal Pendidikan Tinggi, Riset dan Teknologi through a Fundamental Research Grand 2024 (111/E5/PG.02.00PL/2024; 617/LL9/PK.00.PG/2024; 2907/UNIVERAL/LPPM/VI/2024). The authors would like to thank the Kementerian Pendidikan, Kebudayaan, Riset dan Teknologi Indonesia, LLDIKTI Wilayah IX Indonesia dan Lembaga Penelitian dan Pengabdian Kepada Masyarakat Universitas Almarisah Madani Indonesia for providing support.

Declaration of Generative AI in Scientific Writing

This study employed the artificial intelligence (AI) tool ChatGPT to support manuscript writing, including language refinement (improving grammar, sentence structure, and overall readability) and technical writing assistance (providing suggestions for structuring complex technical descriptions more effectively). All AI-assisted processes were critically reviewed by the authors to ensure the integrity and reliability of the results. The final decisions and interpretations presented in this article were made solely by the authors.

CRediT Author Statement

Nur Khairi: Conceptualization; Writing - Original draft preparation. Nursamsiar **Nursamsiar:** Methodology; Softwere Data curation; **Novi Fajar Utami:** Visualization; Investigation. **Syamsu Nur:** Supervision. **Maulita Indrisari:** Writing - Reviewing and Editing. **Marwati Marwati:** Validation.

References

[1] N Khairi, S As'Ad, K Djawad and G Alam. The effectiveness of extract klika streculia populifolia cream on the collagen of albino mice against Ultraviolet B radiation. *Indian Journal of Public Health Research and Development* 2019; **10(1)**, 309.

[2] N Khairi, S As'ad, K Djawad and G Alam. Effects of klika faloak (Sterculia populifolia). *Egyptian Journal of Basic and Clinical Pharmacology* 2019. https://doi.org/10.32527/2019/101408

[3] N Khairi, S As'Ad, K Djawad and G Alam. The determination of antioxidants activity and sunblock Sterculia populifolia extract- based cream. *Pharmaceutical and Biomedical Research* 2018; **4(1)**, 20-26.

[4] N Khairi, N Nursamsiar, NF Utami, M Marwati, S Nur, M Indrisari and S Kursia. Phytochemical profiling and enzyme inhibitory activity of Sterculia populifolia DC stem bark extract and fractions against elastase and tyrosinase. *Narra J* 2025; **5(3)**, e1778.

[5] EF Costa, WV Magalhães and LCD Stasi. Recent advances in herbal-derived products with skin anti-aging properties and cosmetic applications. *Molecules* 2022; **27(21)**, 7518.

[6] G Siquier-Dameto, S Boisnchatic, P Boadas-Vaello and E Verdú. Anti-aging and depigmentation effect of a hyaluronic acid mechanically stabilized complex on human skin explants. *Polymers* 2023; **15(11)**, 2438.

[7] A Fernandes, PM Rodrigues, M Pintado and FK Tavaria. A systematic review of natural products for skin applications: Targeting inflammation, wound healing, and photo-aging. *Phytomedicine* 2023; **115**, 154824.

[8] S Kanwal, S Ahmad, MY Begum, A Siddiqua, H Rao, BA Ghalloo, MN Shahzad, I Ahmad and KR Khan. Chemical profiling, *in-vitro* biological evaluation and molecular docking studies of Ruellia tweediana: An unexplored plant. *Saudi Pharmaceutical Journal* 2024; **32(2)**, 101939.

[9] N Jaradat, M Hawash, MT Qaoud, N Al-Maharik, M Qadi, F Hussein, L Issa, A Saleh, L Saleh and A Jadallah. Biological, phytochemical and molecular docking characteristics of Laurus nobilis L. fresh leaves essential oil from Palestine. *BMC Complementary Medicine and Therapies* 2024; **24(1)**, 223.

[10] S Zolghadri, A Bahrami, MTH Khan, J Munoz-Munoz, F Garcia-Molina, F Garcia-Canovas and AA Saboury. A comprehensive review on tyrosinase inhibitors. *Journal of Enzyme Inhibition and Medicinal Chemistry* 2019; **34(1)**, 279-309.

[11] HAS El-Nashar, MIG El-Din, L Hritcu and OA Eldahshan. Insights on the inhibitory power of flavonoids on tyrosinase activity: A survey from 2016 to 2021. *Molecules* 2021; **26(24)**, 7546.

[12] M Chatatikun, A Tedasen, NC Pattaranggoon, W Palachum, S Chuaijit, A Mudpan, S Pruksaphanrat, S Sohbenalee, K Yamasaki and WK Klangbud. Antioxidant activity, anti-tyrosinase activity, molecular docking studies, and molecular dynamic simulation of active compounds found in nipa palm vinegar. *PeerJ* 2023; **11**, e16494.

[13] L Panzella and A Napolitano. Natural and bioinspired phenolic compounds as tyrosinase inhibitors for the treatment of skin hyperpigmentation: Recent advances. *Cosmetics* 2019; **6(4)**, 57.

[14] K Pohntadavit, S Duangmano, M Osiriphan, N Leksawasdi, C Techapun, N Sumonsiri, SR Sommano, P Rachtanapun, R Nunta and J Khemacheewakul. Tyrosinase inhibitory activity of crude procyanidin extract from green soybean seed and the stability of bioactive compounds in an anti-aging skin care formulation. *Cosmetics* 2024; **11(5)**, 178.

[15] CD Bui, TT Dinh, TT Le, TV Tran, CDM Huynh, TH Le, NT Nguyen, MTT Nguyen, HX Nguyen, TNV Do and H Tran-Van. Anti-tyrosinase activity of Curcuma aromatica ethyl acetate extract: From lead diarylheptanoids to melanogenesis targets. *Beni-Suef University Journal of Basic and Applied Sciences* 2025; **14(1)**, 86.

[16] I Mahdi, P Imbimbo, AB Ortaakarsu, MA Ochieng, WB Bakrim, BE Drissi, MA Ibrahim, MAO Abdelfattah, MF Mahmoud, DM Monti and M Sobeh. Chemical profiling and dermatological and anti-aging properties of Syzygium jambos L. (Alston): Evidence from molecular docking, molecular dynamics, and *in vitro* experiments. *Frontiers in Molecular Biosciences* 2024; **10**, 1331059.

[17] J Lu, Z Zhao, L Pan, H Wu, S Wang, X Tong and S Wu. Hyaluronidase: Structure, mechanism of action, diseases and therapeutic targets. *Molecular Biomedicine* 2025; **6(1)**, 50.

[18] H Yamaguchi, R Yamada, K Lama, UJ Youn, JH Lee and TJ Oh. Integrating LC-MS/MS and *In Silico* methods to uncover bioactive compounds with lipase inhibitory potential in the antarctic moss warnstorfia fontinaliopsis. *Applied Biochemistry and Biotechnology* 2025; **197(4)**, 2734-2756.

[19] S Soltani, RBA Kolsi, N Baccouch, T Michel, N Allouche and HB Salah. LC–MS/MS Profiling, Biological activities and molecular docking studies of simmondsia chinensis leaves. Chinensis Leaves. *Chemistry & Biodiversity* 2025; **22(3)**, e202401833.

[20] R Zhao, E Bruning, D Rossetti, B Starcher, M Seiberg and V Iotsova-Stone. Extracts from Glycine max (soybean) induce elastin synthesis

and inhibit elastase activity. *Experimental Dermatology* 2009; **18(10)**, 883-886.

[21] K Tsukahara, H Nakagawa, S Moriwaki, Y Takema, T Fujimura and G Imokawa. Inhibition of ultraviolet-B-induced wrinkle formation by an elastase-inhibiting herbal extract: Implication for the mechanism underlying elastase-associated wrinkles. *International Journal of Dermatology* 2006; **45(4)**, 460-468.

[22] A García-Villegas, A Rojas-García, MC Villegas-Aguilar, P Fernández-Moreno, Á Fernández-Ochoa, ML Cádiz-Gurrea, D Arráez-Román and A Segura-Carretero. cosmeceutical potential of major tropical and subtropical fruit by-products for a sustainable revalorization. *Antioxidants* 2022; **11(2)**, 203.

[23] N Zulkefli, CNMC Zahari, NH Sayuti, AA Kamarudin, N Saad, HS Hamezah, H Bunawan, SN Baharum, A Mediani, QU Ahmed, AFH Ismail and MN Sarian. Flavonoids as potential wound-healing molecules: Emphasis on Pathways Perspective. *International Journal of Molecular Sciences* 2023; **24(5)**, 4607.

[24] KL Cheong, A Sabir, M Wang, S Zhong and K Tan. Advancements in the extraction, characterization, and bioactive potential of laminaran: A Review. *Foods* 2025; **14(10)**, 1683.

[25] A Mir-Cerdà, O Nuñez, M Granados, S Sentellas and J Saurina. An overview of the extraction and characterization of bioactive phenolic compounds from agri-food waste within the framework of circular bioeconomy. *TrAC Trends in Analytical Chemistry* 2023; **161**, 116994.

[26] G Sliwoski, S Kothiwale, J Meiler and EW Lowe. Computational methods in drug discovery. *Pharmacological Reviews* 2014; **66(1)**, 334-395.

[27] FS Senol Deniz, IE Orhan and H Duman. Profiling cosmeceutical effects of various herbal extracts through elastase, collagenase, tyrosinase inhibitory and antioxidant assays. *Phytochemistry Letters* 2021; **45**, 171-183.

[28] H Mechqoq, S Hourfane, ME Yaagoubi, AE Hamdaoui, JRGDS Almeida, JM Rocha and NE Aouad. Molecular docking, tyrosinase, collagenase, and elastase inhibition activities of argan by-products. *Cosmeticsc* 2022; **9(1)**, 24.

[29] J Widelski, K Gaweł-Bęben, K Czech, E Paluch, O Bortkiewicz, S Kozachok, T Mroczek and P Okińczyc. Extracts from European propolises as potent tyrosinase inhibitors. *Molecules* 2022; **28(1)**, 55.

[30] F Pintus, S Floris, A Fais, B Era, A Kumar, G Gatto, E Uriarte and MJ Matos. Hydroxy-3-phenylcoumarins as multitarget compounds for skin aging diseases: Synthesis, molecular docking and tyrosinase, elastase, collagenase and hyaluronidase inhibition, and sun protection factor. *Molecules* 2022; **27(20)**, 6914.

[31] J Lee, S Moon, Y Hong, D Ahn and H Paik. Anti-elastase and anti-hyaluronidase activity of phosvitin isolated from hen egg yolk. *British Poultry Science* 2020; **61(1)**, 17-21.

[32] C Jiratchayamaethasakul, Y Ding, O Hwang, ST Im, Y Jang, SW Myung, JM Lee, HS Kim, SC Ko and SH Lee. *In vitro* screening of elastase, collagenase, hyaluronidase, and tyrosinase inhibitory and antioxidant activities of 22 halophyte plant extracts for novel cosmeceuticals. *Fisheries and Aquatic Sciences* 2020; **23(1)**, 6.

[33] Y Desmiaty, F Saputri, M Hanafi, R Prastiwi and B Elya. Anti-elastase, anti-tyrosinase and anti-oxidant of rubus fraxinifolius stem methanolic extract. *Pharmacognosy Journal* 2020; **12(2)**, 271-275.

[34] LA Ticona, JS Sánchez-Corral, CDG Martín, SC Jiménez, AL González and CT Estrada. Rubus urticifolius Compounds with Antioxidant Activity, and inhibition potential against Tyrosinase, Melanin, Hyaluronidase, Elastase, and Collagenase. *Pharmaceuticals* 2024; **17(7)**, 937.

[35] IGB Krisnayana, PD Febyani, IAYP Sari and NPL Laksmiani. Molecular docking of lutein as anti-photoaging agent *in silico*. *Pharmacy Reports* 2021; **1(1)**, 15.

[36] NKDP Dewi, KD Suryadewi, DM Fitriari, KL Andini, NPL Laksmiani. Molecular docking of gallic acid as anti-photoaging *in silico*. *Pharmacy Reports* 2021; **1(2)**, 18.

[37] A Akbar, NH Soekamto, Firdaus and Bahrun. Antioxidant of n-hexane, ethyl acetate and methanol extracts of Padina sp with DPPH method. *IOP Conference Series: Earth and Environmental Science* 2021; **800(1)**, 012019.

[38] A Wakeel, SA Jan, I Ullah, ZK Shinwari and M Xu. Solvent polarity mediates phytochemical yield and antioxidant capacity of Isatis tinctoria. *PeerJ* 2019; **7**, e7857.

[39] MQ Lian, WH Chng, J Liang, HQ Yeo, CK Lee, M Belaid, M Tollemeto, MG Wacker, B Czarny and G Pastorin. Plant-derived extracellular vesicles: Recent advancements and current challenges on their use for biomedical applications. *Journal of Extracellular Vesicles* 2022; **11(12)**, e12283.

[40] AG Atanasov, B Waltenberger, EM Pferschy-Wenzig, T Linder, C Wawrosch, P Uhrin, V Temml, L Wang, S Schwaiger, EH Heiss, JM Rollinger, D Schuster, JM Breuss, V Bochkov, MD Mihovilovic, B Kopp, R Bauer, VM Dirsch and H Stuppner. Discovery and resupply of pharmacologically active plant-derived natural products: A review. *Biotechnology Advances* 2015; **33(8)**, 1582-1614.

[41] M Syukur, MS Prahasiwi, N Nurkhasanah, S Yuliani, Y Purwaningsih and E Indriyanti. Profiling of active compounds of extract ethanol, n-Hexane, ethyl acetate and fraction ethanol of star anise (Illicium verum Hook. f.) and determination of total flavonoids, total phenolics and their potential as antioxidants. *Science and Technology Indonesia* 2023; **8(2)**, 219-226.

[42] A Akbar, NH Soekamto, Firdaus and Bahrun. Total phenolics and flavonoids level of n-hexane, ethyl acetate and methanol extracts of Sargassum sp. along with their antioxidant activity by DPPH method. *AIP Conference Proceedings* 2022; **2638**, 060009.

[43] CD Bui, TT Dinh, TT Le, TV Tran, CDM Huynh, TH Le, NT Nguyen, MTT Nguyen, HX Nguyen, TNV Do and H Tran-Van. Anti-tyrosinase activity of Curcuma aromatica ethyl acetate extract: From lead diarylheptanoids to melanogenesis targets. *Beni-Suef University Journal of Basic and Applied Sciences* 2025; **14(1)**, 86.

[44] L Panzella and A Napolitano. Natural and Bioinspired Phenolic Compounds as Tyrosinase Inhibitors for the Treatment of Skin Hyperpigmentation: Recent Advances. *Cosmetics* 2019; **6(4)**, 57.

[45] T Pillaiyar, M Manickam and V Namasivayam. Skin whitening agents: Medicinal chemistry perspective of tyrosinase inhibitors. *Journal of Enzyme Inhibition and Medicinal Chemistry* 2017; **32(1)**, 403-425.

[46] C Horng, H Wu, N Chiang, C Lee, YS Huang, HY Wang, JS Yang and FA Chen. Inhibitory effect of burdock leaves on elastase and tyrosinase activity. *Experimental and Therapeutic Medicine* 2017; **14(4)**, 3247-3252.

[47] YS Lin, HJ Chen, JP Huang, PC Lee, CR Tsai, TF Hsu and WY Huang. Kinetics of tyrosinase inhibitory activity using vitis vinifera leaf extracts. *BioMed Research International* 2017; **2017**, 5232680.

[48] H Maamoun, G Rabie, I Shaker, B Alaidaroos and A El-Sayed. Biochemical properties of tyrosinase from aspergillus terreus and penicillium copticola; undecanoic acid from aspergillus flavus, an endophyte of moringa oleifera, is a novel potent tyrosinase inhibitor. *Molecules* 2021; **26(5)**, 1309.

[49] F Yang, Y Hu, M Wu, M Guo and H Wang. Biologically active components and skincare benefits of rice fermentation products: A review. *Cosmetics* 2025; **12(1)**, 29.

[50] CH Eun, MS Kang and IJ Kim. Elastase/Collagenase inhibition compositions of citrus unshiu and its association with phenolic content and anti-oxidant activity. *Applied Sciences* 2020; **10(14)**, 4838.

[51] S Ahmad, M Saleem, N Riaz, Y Lee, R Diri, A Noor, D Almasri, A Bagalagel and MF Elsebai. The natural polypeptides as significant elastase inhibitors. *Frontiers in Pharmacology* 2020; **11**, 688.

[52] N Morisaki, S Moriwaki, Y Sugiyama-Nakagiri, K Haketa, Y Takema and G Imokawa. Neprilysin is identical to skin fibroblast elastase. *Journal of Biological Chemistry* 2010; **285(51)**, 39819-39827.

[53] H Khojah, SR Ahmed, SY Alharbi, KK AlSabeelah, HY Alrayyes, KB Almusayyab, SR Alrawiliy, RM Alshammari, and S Qasim. Skin anti-aging potential of Launaea procumbens extract: Antioxidant and enzyme inhibition activities supported by ADMET and molecular

docking studies. *Saudi Pharmaceutical Journal* 2024; **32(7)**, 102107.

[54] I Mahdi, P Imbimbo, AB Ortaakarsu, MA Ochieng, WB Bakrim, BE Drissi, MA Ibrahim, MAO Abdelfattah, MF Mahmoud, DM Monti and M Sobeh. Chemical profiling and dermatological and anti-aging properties of Syzygium jambos L. (Alston): Evidence from molecular docking, molecular dynamics, and *in vitro* experiments. *Frontiers in Molecular Biosciences* 2024; **10**, 1331059.

[55] F Pintus, S Floris, A Fais, B Era, A Kumar, G Gatto and E Uriarte. Hydroxy-3-Phenylcoumarins as Multitarget Compounds for Skin Aging Diseases: Synthesis, Molecular Docking and Tyrosinase, Elastase, Collagenase and Hyaluronidase Inhibition, and Sun Protection Factor. *Molecules* 2022; **27(20)**, 6914.

[56] FSS Deniz, RE Salmas, E Emerce, IIT Cankaya, HS Yusufoglu and IE Orhan. Evaluation of collagenase, elastase and tyrosinase inhibitory activities of Cotinus coggygria Scop. through *in vitro* and *in silico* approaches. *South African Journal of Botany* 2020; **132**, 277-288.

[57] JH Lee, SH Moon, Y Hong, DU Ahn and HD Paik. Anti-elastase and anti-hyaluronidase activity of phosvitin isolated from hen egg yolk. *British Poultry Science* 2020; **61(1)**, 17-21.

[58] S Abdillah, G Wijiyanti, M Setiawan, S Noor and M Nurilmala. *In vitro* anti-tyrosinase and anti-elastase activity of collagen from sea cucumber (Holothuria leucospilota). *African Journal of Biotechnology* 2017; **16(15)**, 771-776.

[59] A Vardhani, M Jufri, E Purwaningsih. Potency of γ-oryzanol-rich black rice bran (oryza sativa l. indica) extract for tyrosinase inhibition. *International Journal of Pharmacy and Pharmaceutical Sciences* 2020; **12(5)**, 85-89.

[60] MC Kwon, WY Choi, YC Seo, JS Kim, CS Yoon, HW Lim, HS Kim, J Ahn and HY Lee. Enhancement of the Skin-protective activities of centella asiatica L. urban by a nano-encapsulation process. *Journal of Biotechnology* 2012; **157(1)**, 100-106.